

# Blind reconstruction of sparse images with unknown point spread function

Kyle Herrity<sup>a</sup>, Raviv Raich,<sup>b</sup> and Alfred O. Hero III<sup>a</sup>

<sup>a</sup>Department of EECS, University of Michigan, Ann Arbor, MI 48109-2122

<sup>b</sup>School of EECS, Oregon State University, Corvallis, OR 97331-5501

## ABSTRACT

We consider the image reconstruction problem when the original image is assumed to be sparse and when partial knowledge of the point spread function (PSF) is available. In particular, we are interested in recovering the magnetization density given magnetic resonance force microscopy (MRFM) data, and we present an iterative alternating minimization algorithm (AM) to solve this problem. A smoothing penalty is introduced on allowable PSFs to improve the reconstruction. Simulations demonstrate its performance in reconstructing both the image and unknown point spread function. In addition, we develop an optimization transfer approach to solving a total variation (TV) blind deconvolution algorithm presented in a paper by Chan and Wong. We compare the performance of the AM algorithm to the blind TV algorithm as well as to a TV based majorization-minimization algorithm developed by Figueiredo *et al.*

**Keywords:** Image restoration, Blind deconvolution, Magnetic resonance force microscopy, Sparseness regularization, Optimization transfer, Total variation

## 1. INTRODUCTION

Image restoration is an integral component of many image processing applications; the goal is to recover the original image from a degraded observation. The topic of image deconvolution has been studied in detail.<sup>1</sup> Ideally, the point spread function (PSF) is known *a priori* and linear image restoration algorithms attempt to invert it. However, in most systems, the PSF is unknown, or we may have partial information about it. In such cases, we try to estimate both the true PSF and the original image in a process referred to as *blind image reconstruction*. Common techniques for reconstructing images include Maximum-Likelihood (ML) approaches and the classical method of Least-Squares (LS), when the statistical properties of the noise are at hand. In both cases, we are lead to ill-posed problems and must ensure that appropriate regularizing measures are taken.

This paper caters toward the application of Magnetic Resonance Force Microscopy (MRFM), which is a relatively new imaging technology, capable of attometer (1 millionth of a nanometer) spatial resolution, and possibly atomic-scale resolution in the future. MRFM has the potential to observe protein structures otherwise unobservable via other existing technologies, including X-ray crystallography and protein nuclear magnetic resonance spectroscopy (also known as protein NMR).

Our consideration of sparse images in the problem statement lends itself well to molecular imaging applications, where most of the image space is empty, and only a few spatial locations are occupied by atoms. By modeling sparsity, we hope to gain improvements in the reconstruction performance of our algorithm. We will also assume that partial knowledge of the PSF of the MRFM system is available. From the physical nature of the MRFM experiment, it is sensible to restrict our focus of attention to a space of PSFs which have certain smooth characteristics to be defined more precisely later.

We consider a parametric model of the PSF,<sup>2,3</sup>  $h(\theta)$ , which includes parameters such as the externally applied magnetic field,  $B_{\text{ext}}$ , under appropriate setup conditions (See Table 1). We then linearize about a nominal PSF,

---

Further author information: (Send correspondence to A.O.H.)

K.H.: E-mail: kherrity@umich.edu

R.R.: E-mail: raich@eeecs.oregonstate.edu

A.O.H.: E-mail: hero@umich.edu

i.e.  $h(\theta) = h(\theta_0) + h'(\theta)(\theta - \theta_0)$  for a given choice of parameters, and are thus able to recast the norm of the error as a non-isotropic quadratic criterion. We have developed an alternating minimization algorithm in a paper submitted to ICASSP that addresses these issues.<sup>4</sup>

Table 1. MRFM Parameters used to illustrate the MRFM psf

| Description                                     | Name             | Value                  |
|---|------------------|------------------------|
| Amplitude of external magnetic field            | $B_{\text{ext}}$ | $2 \times 10^4$ G      |
| Value of $B_{\text{mag}}$ in the resonant slice | $B_{\text{res}}$ | $2.25 \times 10^4$ G   |
| Radius of tip when modeled as a sphere          | $R_0$            | 2 nm                   |
| Distance from tip to sample                     | $d$              | 2 nm                   |
| Cantilever tip moment                           | $m$              | $5.70 \times 10^4$ emu |
| Peak cantilever swing                           | $x_{\text{pk}}$  | 0.033 nm               |
| Maximum magnetic field gradient                 | $G_{\text{max}}$ | 610 G/nm               |

Satisfactory image reconstruction results have been obtained by Chan and Wong<sup>5</sup> by using a Total Variation (TV) based method in an alternating minimization blind deconvolution algorithm. The authors make minimal assumptions on the PSF, and state their motivation for using TV is due to the fact that PSFs can have edges. We have developed an algorithm based on Chan and Wong’s algorithm using optimization transfer techniques, and we compare its performance against the AM algorithm.

### 1.1 A brief overview of MRFM

MRFM was proposed as a means to detect images at the single-spin level, with the hope of one day achieving atomic scale resolution capabilities. The technology of MRFM combines scanning probe microscopy with magnetic resonance imaging (MRI), giving it the ability to visualize subsurface structures in three dimensions with very high resolution.<sup>6</sup>

The basic apparatus of the MRFM experiment consists of a magnetic tip at the end of a vertically oriented ultrasensitive silicon cantilever. Sample spins couple resonantly with an applied rf field if only if they are located within a resonant slice. The resonant slice is created by the magnetic tip of the force microscope cantilever. Magnetic resonance is detected by the magnetic force exerted between the magnetic spin and the sample. As the cantilever scans over the surface of the sample recording the MRFM signal, the distribution of spins of the sample can be reconstructed. In a landmark experiment in 2004, IBM researchers were able to detect a single electron spin using the ‘interrupted OSCAR’ or iOSCAR protocol.<sup>7</sup>

Techniques from signal processing will prove to be vital in the realization of MRFM as a viable molecular imaging technology. We hope that the image reconstruction formulations put forth in this paper will aid in this effort.

## 2. PROBLEM STATEMENT

The problem we will be considering is a linear observation model of the form

$$\mathbf{y} = \mathbf{H}\mathbf{x} + \mathbf{n}, \tag{1}$$

where  $\mathbf{H} \in \mathbb{R}^{m \times n}$  is the observation or blurring matrix,  $\mathbf{x} \in \mathbb{R}^n$  denotes the original image, and  $\mathbf{n} \in \mathbb{R}^m$  represents the noise. In this paper, we consider the case where the noise is a sample of zero-mean Gaussian noise with covariance  $\sigma^2\mathbf{I}$ , where  $\mathbf{I}$  is the identity matrix. When  $\mathbf{H}$  describes a convolution, it will possess a block Toeplitz structure, and if we assume that we are zero-padding the image appropriately, the matrix  $\mathbf{H}$  will be circulant, and hence diagonalizable by the discrete Fourier transform (DFT) matrix. We will assume this nice structural property on  $\mathbf{H}$ , which will allow for simplified derivations later on.

For a detailed presentation of our sparse alternating minimization algorithm (AM), one should consult our earlier work.<sup>4</sup> For completeness, however, we will present the basic formulation of the algorithm. We start by

recalling that the maximum likelihood (ML) estimator of the image  $x$ , when  $\mathbf{n}$  is a zero-mean white Gaussian noise vector, is the minimizer of the cost function

$$J(\mathbf{x}) = \|\mathbf{H}\mathbf{x} - \mathbf{y}\|^2. \quad (2)$$

Note that we are using  $\|\cdot\|$  to denote the standard  $l_2$  norm  $\|\cdot\|_2$ , where  $\|\mathbf{x}\|_2 \triangleq \sum_{i=1}^n x_i^2$ . Other norms such as the  $l_1$  norm, defined as  $\|\mathbf{x}\|_1 \triangleq \sum_{i=1}^n |x_i|$ , will be written explicitly using a subscript. Because we assume partial knowledge of the MRFM PSF, we will express  $\mathbf{H}$  as

$$\mathbf{H} = \mathbf{H}_0 + \epsilon\mathbf{\Delta}, \quad (3)$$

where  $\mathbf{H}_0$  may be thought of as our nominal PSF, or the part of  $\mathbf{H}$  that we know, while the unknown portion of  $\mathbf{H}$  is contained in the  $\epsilon\mathbf{\Delta}$  term. Additionally, we assume that

$$\|\mathbf{\Delta}\|_{\mathbf{W}} \triangleq \|\mathbf{W}\mathbf{\Delta}\| \leq \epsilon, \quad (4)$$

where  $\mathbf{W}$  is a non-identity smoothing matrix. The  $l_2$  norm of a matrix  $\mathbf{C}$  will be defined as  $\|\mathbf{C}\| \triangleq \max_{\mathbf{s} \neq \mathbf{0}} \frac{\|\mathbf{C}\mathbf{s}\|}{\|\mathbf{s}\|}$ . Equation (4) is where we impose the constraint that the true PSF is in some sense a ‘‘smooth’’ extension of the nominal PSF, which is reasonably justified by the physical setup of the MRFM experiment. We will later make use of this constraint in our objective function which AM solves.

We can now express the cost function in (2) as

$$J(\mathbf{x}) = \|(\mathbf{H}_0 + \epsilon\mathbf{\Delta})\mathbf{x} - \mathbf{y}\|^2. \quad (5)$$

In order to remove the dependence of  $\mathbf{\Delta}$ , we study the minimax criterion. In other words, we seek the  $x$  which minimizes Equation (5) for the worst case scenario on  $\mathbf{\Delta}$ . Thus, our new cost function becomes

$$J(\mathbf{x}) = \max_{\mathbf{\Delta}} \|(\mathbf{H}_0 + \epsilon\mathbf{\Delta})\mathbf{x} - \mathbf{y}\|^2 \quad \text{s.t.} \quad \|\mathbf{\Delta}\|_{\mathbf{W}} \leq \epsilon. \quad (6)$$

A few notational comments should be mentioned. By the commutative property of convolution, and because we view the linear operator  $\mathbf{H}$  acting on  $\mathbf{x}$  to be the convolution operator, we have that  $\mathbf{H}\mathbf{x} = \mathbf{X}\mathbf{h}$ , where  $\mathbf{X}$  is assumed to be circulant and thus diagonalizable by the DFT matrix, which we will denote as  $\mathbf{F}$ . We will write

$$\mathbf{X} = \mathbf{F} \text{diag}(\mathbf{F}^H \mathbf{x}) \mathbf{F}^H, \quad (7)$$

where  $\mathbf{F}^H$  denotes the conjugate transpose of  $\mathbf{F}$ . Similarly,

$$\begin{aligned} \mathbf{H} &= \mathbf{F} \text{diag}(\mathbf{F}^H \mathbf{h}) \mathbf{F}^H \\ \mathbf{\Delta} &= \mathbf{F} \text{diag}(\mathbf{F}^H \delta) \mathbf{F}^H. \end{aligned}$$

It should be noted that this treatment yields computational savings, as matrix multiplication is represented by convolutions and may be efficiently implemented via the FFT.

## 2.1 The sparsity and smoothness constraints

A critical notion in this paper is that of sparsity. Recall that the sparseness of an image  $\mathbf{x}$  is the number of nonzero elements of  $\mathbf{x}$ . More precisely, the sparsity may be defined in terms of the  $l_0$  norm as

$$\|\mathbf{x}\|_0 \triangleq \sum_{i=1}^n I(\mathbf{x}_i \neq 0), \quad (8)$$

where  $I(\cdot)$  is the indicator function. As mentioned in the introduction, the AM algorithm is tailored to the situation where one expects sparse images; i.e. the images MRFM acquires are inherently sparse by nature. We might therefore be interested in solving the following minimization problem for a given  $\tilde{\mathbf{H}}$  function

$$\min_{\mathbf{x}} \|\tilde{\mathbf{H}}\mathbf{x} - \mathbf{y}\|^2 \quad \text{s.t.} \quad \|\mathbf{x}\|_0 \leq p. \quad (9)$$

This problem is highly combinatorial, with a total of  $\sum_{i=0}^p \binom{n}{i}$  possible solutions, and in fact, it can be shown to be NP-hard.<sup>8,9</sup> By convexifying the sparsity constraint, we can employ a well-known method for solving problems of this type known as convex relaxation. This amounts to replacing the  $l_0$  constraint with an  $l_1$  constraint, and under certain conditions on  $\tilde{\mathbf{H}}$ , identical solutions may be obtained. Using the method of Lagrange multipliers, we arrive at the minimization problem

$$\hat{\mathbf{x}} = \arg \min_{\mathbf{x}} \|\tilde{\mathbf{H}}\mathbf{x} - \mathbf{y}\|^2 + \lambda \|\mathbf{x}\|_1. \quad (10)$$

We consider approaching the solution of (10) by utilizing optimization transfer techniques described in an earlier paper.<sup>10</sup> If we denote our optimality criterion by  $F(\mathbf{x})$ , the idea is to find a non-negative function  $Q(\mathbf{x}, \mathbf{x}')$ , i.e.,  $Q(\mathbf{x}, \mathbf{x}') \geq 0$ , and such that  $Q(\mathbf{x}, \mathbf{x}') = 0$  if and only if  $\mathbf{x} = \mathbf{x}'$ . Then the iterations

$$\hat{\mathbf{x}}^{(n+1)} = \arg \min_{\mathbf{x}} F(\mathbf{x}) + Q(\mathbf{x}, \hat{\mathbf{x}}^{(n)}), \quad (11)$$

are such that  $F(\hat{\mathbf{x}}^{(n)})$  is a non-increasing function of  $n$ . Let

$$F(\mathbf{x}) = \|\tilde{\mathbf{H}}\mathbf{x} - \mathbf{y}\|^2 + \lambda \|\mathbf{x}\|_1, \quad (12)$$

as in (10). We introduce a surrogate function for the  $l_1$  norm in the spirit of work by Figueiredo and Nowak.<sup>11</sup> Observe that for all  $x, x'$  in  $\mathbb{R}$ , where  $x' \neq 0$ ,

$$|x| \leq \frac{x^2}{2|x'|} + \frac{|x'|}{2}. \quad (13)$$

Thus, for all  $\mathbf{x}'$  whose components are nonzero,

$$F(\mathbf{x}) \leq \|\tilde{\mathbf{H}}\mathbf{x} - \mathbf{y}\|^2 + \frac{\lambda}{2} (\mathbf{x}^T \text{diag}(\frac{1}{|\mathbf{x}'|}) \mathbf{x} + \|\mathbf{x}'\|_1). \quad (14)$$

Additional care must be taken when one or more of the components of  $\mathbf{x}'$  is zero. Therefore, we set

$$\hat{\mathbf{x}}^{(n+1)} = \arg \min_{\mathbf{x}} \|\tilde{\mathbf{H}}\mathbf{x} - \mathbf{y}\|^2 + \frac{\lambda}{2} (\mathbf{x}^T \text{diag}(\frac{1}{|\hat{\mathbf{x}}^{(n)}|}) \mathbf{x}). \quad (15)$$

By differentiating with respect to  $\mathbf{x}$ , it can be shown that

$$\hat{\mathbf{x}}^{(n+1)} = \left( \tilde{\mathbf{H}}^T \tilde{\mathbf{H}} + \lambda \cdot \text{diag}(\frac{1}{|\hat{\mathbf{x}}^{(n)}|}) \right)^{-1} \tilde{\mathbf{H}}^T \mathbf{y}. \quad (16)$$

Assuming the inverse above exists, we compute it via a series of Landweber iterations. As the sparsity increases, the computation time of the iterates in Equation (16) decreases rapidly.

As mentioned before, the other constraint we are enforcing is through a smoothness penalty on allowable PSFs. Combining the smoothness and sparsity constraints and appealing to the notational conventions set out in Section 2 leads to the regularized cost function<sup>4</sup>

$$J(\mathbf{x}; \delta) = \|\mathbf{X}(\mathbf{h}_0 + \epsilon\delta) - \mathbf{y}\|^2 \quad \text{s.t.} \quad \|\mathbf{x}\|_1 \leq \tilde{p} \quad \text{and} \quad \|\mathbf{W}\delta\|^2 \leq \epsilon. \quad (17)$$

## 2.2 AM algorithm

We propose an alternating algorithm (AM) to solve the regularized cost function (17). It proceeds as follows<sup>4</sup>

### AM algorithm

1. Initialize  $\mathbf{x}^{(0)}$  to a suitable first estimate (e.g. via thresholding),  $\mathbf{y}^{(0)} = \mathbf{y}$ , and  $\mathbf{H}^{(0)} = \mathbf{H}_0$ .

2. Update  $\mathbf{x}^{(n)}$  by solving

$$\mathbf{x}^{(n+1)} = \arg \min_{\mathbf{x}} \|\mathbf{H}^{(n)}\mathbf{x} - \mathbf{y}^{(n)}\|^2 \quad \text{s.t.} \quad \|\mathbf{x}\|_1 \leq p.$$

3. Update  $\mathbf{H}^{(n)}$  and  $\mathbf{y}^{(n)}$  by solving

$$\arg \max_{\mathbf{H}} \|y - \mathbf{H}\mathbf{x}^{(n)}\|^2 \quad \text{s.t.} \quad \|\mathbf{W}\Delta\|^2 \leq \epsilon.$$

This leads to the updates

$$\begin{aligned} \mathbf{H}^{(n+1)} &= \left( \mathbf{I} + \epsilon^2 \mathbf{X}^{(n)} (\gamma \mathbf{W}^T \mathbf{W} - \epsilon^2 \mathbf{X}^{(n)T} \mathbf{X}^{(n)})^{-1} \mathbf{X}^{(n)T} \right) \mathbf{H}_0, \\ \mathbf{y}^{(n+1)} &= \left( \mathbf{I} + \epsilon^2 \mathbf{X}^{(n)} (\gamma \mathbf{W}^T \mathbf{W} - \epsilon^2 \mathbf{X}^{(n)T} \mathbf{X}^{(n)})^{-1} \mathbf{X}^{(n)T} \right) \mathbf{y}. \end{aligned}$$

4. When the stopping criterion is met, output the estimated image  $\mathbf{x}^{(n)}$  and the estimated PSF  $\mathbf{H}^{(n)}$ .

### 2.3 Reconstructing the PSF

An alternative approach is to set the smoothing penalty  $\gamma$  sufficiently high in AM. After the completion of the algorithm, with the reconstructed image  $\hat{\mathbf{x}}$  fixed, we solve the minimization problem as before to recover  $\mathbf{H}$ .

$$\arg \min_{\mathbf{H}} \|\hat{\mathbf{X}}\mathbf{h} - \mathbf{y}\|^2 + \tilde{\gamma} \|\mathbf{W}\delta\|^2, \quad (18)$$

where  $\tilde{\gamma}$  is the smoothing penalty we enforce. It should be emphasized that while we reconstruct  $\mathbf{H}$  this way, we do not substitute the reconstructed  $\mathbf{H}$  back into the algorithm.

## 3. A TOTAL VARIATION APPROACH

We formulate the blind deconvolution problem using total variation as in the paper by Chan and Wong,<sup>5</sup> as

$$\min_{\mathbf{x}, \mathbf{h}} f(\mathbf{x}, \mathbf{h}) = \frac{1}{2} \min_{\mathbf{x}, \mathbf{h}} \|\mathbf{h} * \mathbf{x} - \mathbf{y}\|^2 + \lambda_1 \int_{\Omega} |\nabla \mathbf{x}| + \lambda_2 \int_{\Omega} |\nabla \mathbf{h}|, \quad (19)$$

where  $\mathbf{x}$  is the image,  $\mathbf{h}$  is the PSF,  $\mathbf{y}$  is the noisy and blurred image, and  $\lambda_1$  and  $\lambda_2$  are the regularization parameters which measure the trade off between a good fit and the regularity of the solutions  $\mathbf{x}$  and  $\mathbf{h}$ . Chan and Wong implement a fixed point (FP) algorithm to solve (19). The authors first linearize the nonlinear PDEs arising from the first order optimality conditions by lagging the diffusive coefficients  $\frac{1}{|\nabla \mathbf{h}^{n+1}|}$  and  $\frac{1}{|\nabla \mathbf{x}^{n+1}|}$  by one iteration and then applying FP methods to solve linear problems for  $\mathbf{h}^{n+1}$  and  $\mathbf{x}^{n+1}$  in an alternating algorithm. Unfortunately, we were not able to implement the same version of the algorithm in Chan and Wong's paper. Therefore, we decided to try a different approach and solve (19) by using optimization transfer techniques similar to the ones we have developed in our original problem formulation and to those in a paper by Figueiredo *et al.*<sup>12</sup> One advantage this technique yields is a monotonically decreasing objective function, which cannot be guaranteed by Chan and Wong's method.

Letting  $\mathbf{v} := \left[ \frac{\partial \mathbf{x}}{\partial x} \quad \frac{\partial \mathbf{x}}{\partial y} \right]^T$ , we have

$$\iint |\nabla \mathbf{x}| \, dx dy = \iint \sqrt{\mathbf{v}^T \mathbf{v}} \, dx dy,$$

and

$$\sqrt{\mathbf{v}^T \mathbf{v}} = \sqrt{(\mathbf{v}' + \Delta \mathbf{v})^T (\mathbf{v}' + \Delta \mathbf{v})} \quad (20)$$

$$= \sqrt{\mathbf{v}'^T \mathbf{v}' + 2(\Delta \mathbf{v})^T \mathbf{v}' + \Delta \mathbf{v}^T \Delta \mathbf{v}} \quad (21)$$

$$\leq \sqrt{\mathbf{v}'^T \mathbf{v}'} + \frac{1}{2} \cdot \frac{2(\Delta \mathbf{v})^T \mathbf{v}' + \Delta \mathbf{v}^T \Delta \mathbf{v}}{\sqrt{\mathbf{v}'^T \mathbf{v}'}} \quad (22)$$

$$= \frac{\mathbf{v}'^T \mathbf{v}'}{\|\mathbf{v}'\|_2} + \frac{1}{2} \cdot \frac{(\mathbf{v} - \mathbf{v}')^T (\mathbf{v} - \mathbf{v}')}{\|\mathbf{v}'\|_2} \quad (23)$$

$$= \frac{1}{2} \left[ \frac{\mathbf{v}^T \mathbf{v}}{\|\mathbf{v}'\|_2} + \frac{\mathbf{v}'^T \mathbf{v}'}{\|\mathbf{v}'\|_2} \right] = \frac{1}{2} \left[ \frac{\mathbf{v}^T \mathbf{v}}{\|\mathbf{v}'\|_2} + \|\mathbf{v}'\|_2 \right], \quad (24)$$

where  $\Delta \mathbf{v} := \mathbf{v} - \mathbf{v}'$ . Thus,

$$\iint |\nabla \mathbf{x}| \, dxdy \leq \frac{1}{2} \iint \left( \frac{\mathbf{v}^T \mathbf{v}}{\|\mathbf{v}'\|_2} + \|\mathbf{v}'\|_2 \right) \, dxdy.$$

Similarly, if we let  $\mathbf{r} := \left[ \frac{\partial \mathbf{h}}{\partial x} \ \frac{\partial \mathbf{h}}{\partial y} \right]^T$ , then

$$\iint |\nabla \mathbf{h}| \, dxdy \leq \frac{1}{2} \iint \left( \frac{\mathbf{r}^T \mathbf{r}}{\|\mathbf{r}'\|_2} + \|\mathbf{r}'\|_2 \right) \, dxdy.$$

So,

$$f(\mathbf{x}, \mathbf{h}) \leq \frac{1}{2} \|\mathbf{h} * \mathbf{x} - \mathbf{y}\|^2 + \frac{\lambda_1}{2} \iint \left( \frac{\mathbf{v}^T \mathbf{v}}{\|\mathbf{v}'\|_2} + \|\mathbf{v}'\|_2 \right) \, dxdy + \frac{\lambda_2}{2} \iint \left( \frac{\mathbf{r}^T \mathbf{r}}{\|\mathbf{r}'\|_2} + \|\mathbf{r}'\|_2 \right) \, dxdy.$$

We therefore want to find  $\hat{\mathbf{x}}$ , and  $\hat{\mathbf{h}}$  such that

$$\hat{\mathbf{x}}, \hat{\mathbf{h}} = \arg \min_{\mathbf{x}, \mathbf{h}} \|\mathbf{h} * \mathbf{x} - \mathbf{y}\|^2 + \lambda_1 \iint \frac{\mathbf{x}_x^2 + \mathbf{x}_y^2}{\sqrt{\mathbf{x}'_x^2 + \mathbf{x}'_y^2}} \, dxdy + \lambda_2 \iint \frac{\mathbf{h}_x^2 + \mathbf{h}_y^2}{\sqrt{\mathbf{h}'_x^2 + \mathbf{h}'_y^2}} \, dxdy.$$

Discretizing the above discussion, and using a first order difference approximation of the derivative, (where we denote  $D_x \mathbf{x}$  as the derivative of the image with respect to  $x$ ). For ease of notation, if we let

$$w_{ij}^x := \frac{1}{\sqrt{[D_x \mathbf{x}']_{ij}^2 + [D_y \mathbf{x}']_{ij}^2}},$$

then we can write

$$\begin{aligned} f(\mathbf{x}, \mathbf{h}) &\leq \|\mathbf{H}\mathbf{x} - \mathbf{y}\|^2 + (\mathbf{x} - \mathbf{x}')^T (s_h \mathbf{I} - \mathbf{H}^T \mathbf{H}) (\mathbf{x} - \mathbf{x}') \\ &\quad + \lambda_1 \sum_i \sum_j w_{ij}^x ([D_x \mathbf{x}]_{ij}^2 + [D_y \mathbf{x}]_{ij}^2) \\ &\quad + \lambda_2 \sum_i \sum_j w_{ij}^h ([D_x \mathbf{h}]_{ij}^2 + [D_y \mathbf{h}]_{ij}^2), \end{aligned} \tag{25}$$

where  $s_h > \lambda_{\max}(\mathbf{H})$ , and  $\mathbf{H}\mathbf{x}$  is the matrix-vector representation for the convolution  $\mathbf{h} * \mathbf{x}$ . Observing that we can express

$$\sum_i \sum_j w_{ij}^x ([D_x \mathbf{x}]_{ij}^2 + [D_y \mathbf{x}]_{ij}^2) = \mathbf{x}^T \mathbf{A}(\mathbf{x}) \mathbf{x},$$

where  $\mathbf{A}(\mathbf{x})$  is defined as

$$\mathbf{A}(\mathbf{x}) := [(\mathbf{M} - \mathbf{I})^T \otimes \mathbf{I}] \text{diag}(\mathbf{W}(\mathbf{x})) [(\mathbf{M} - \mathbf{I}) \otimes \mathbf{I}] + [\mathbf{I} \otimes (\mathbf{M} - \mathbf{I})^T] \text{diag}(\mathbf{W}(\mathbf{x})) [\mathbf{I} \otimes (\mathbf{M} - \mathbf{I})],$$

where the elements of  $\text{diag}(\mathbf{W}(\mathbf{x}))$  are the  $w_{ij}^x$  defined earlier (we can define  $\mathbf{A}(\mathbf{h})$  and  $\mathbf{W}(\mathbf{h})$  analogously),  $\mathbf{M}$  is the matrix with ones on its superdiagonal and zeros everywhere else, and  $\otimes$  is the Kronecker product. We then arrive at

$$f(\mathbf{x}, \mathbf{h}) \leq \|\mathbf{H}\mathbf{x} - \mathbf{y}\|^2 + (\mathbf{x} - \mathbf{x}')^T (s_h \mathbf{I} - \mathbf{H}^T \mathbf{H}) (\mathbf{x} - \mathbf{x}') + \lambda_1 \mathbf{x}^T \mathbf{A}(\mathbf{x}) \mathbf{x} + \lambda_2 \mathbf{h}^T \mathbf{A}(\mathbf{h}) \mathbf{h}.$$

If  $\rho_x > \lambda_{\max}(\mathbf{A}(\mathbf{x}))$ , then

$$(\mathbf{x} - \mathbf{x}')^T (\rho_x \mathbf{I} - \mathbf{A}(\mathbf{x})) (\mathbf{x} - \mathbf{x}') \quad \forall (\mathbf{x} - \mathbf{x}') \neq 0.$$

From now on, we will simply write  $\mathbf{A}(\mathbf{x})$  or  $\mathbf{A}(\mathbf{h})$  as  $\mathbf{A}$ , where it will be clear from the context which  $\mathbf{A}$  we mean. Thus,

$$\mathbf{x}^T \mathbf{A} \mathbf{x} < \underbrace{\rho_h \|\mathbf{x} - \mathbf{x}'\|^2 + 2\mathbf{x}'^T \mathbf{A} \mathbf{x} - \mathbf{x}'^T \mathbf{A} \mathbf{x}'}_{:=G(\mathbf{x}, \mathbf{x}')}.$$

So we have

$$f(\mathbf{x}, \mathbf{h}) < \|\mathbf{H}\mathbf{x} - \mathbf{y}\|^2 + (\mathbf{x} - \mathbf{x}')^T (s_h \mathbf{I} - \mathbf{H}^T \mathbf{H})(\mathbf{x} - \mathbf{x}') + \lambda_1 G(\mathbf{x}, \mathbf{x}') + \lambda_2 G(\mathbf{h}, \mathbf{h}'). \quad (26)$$

If we denote  $R(\mathbf{x}, \mathbf{h}, \mathbf{x}', \mathbf{h}')$  as the right-hand-side of (26), and treat  $\mathbf{h}$ ,  $\mathbf{x}'$  and  $\mathbf{h}'$  as constants, differentiating with respect to  $\mathbf{x}$  yields

$$\frac{\partial}{\partial \mathbf{x}} R = \frac{\partial}{\partial \mathbf{x}} [\|\mathbf{H}\mathbf{x} - \mathbf{y}\|^2 + s_h \|\mathbf{x} - \mathbf{x}'\|^2 - (\mathbf{x}^T \mathbf{H}^T \mathbf{H} \mathbf{x} - 2\mathbf{x}^T \mathbf{H}^T \mathbf{H} \mathbf{x}' + \mathbf{x}'^T \mathbf{H}^T \mathbf{H} \mathbf{x}')] + \lambda_1 \frac{\partial}{\partial \mathbf{x}} G(\mathbf{x}, \mathbf{x}') \quad (27)$$

$$= 2\mathbf{H}^T (\mathbf{H}\mathbf{x} - \mathbf{y}) + 2s_h (\mathbf{x} - \mathbf{x}') - 2\mathbf{H}^T \mathbf{H} \mathbf{x} + 2\mathbf{H}^T \mathbf{H} \mathbf{x}' + \lambda_1 \frac{\partial}{\partial \mathbf{x}} G(\mathbf{x}, \mathbf{x}'). \quad (28)$$

But

$$\frac{\partial}{\partial \mathbf{x}} G(\mathbf{x}, \mathbf{x}') = 2\rho_x (\mathbf{x} - \mathbf{x}') + 2\mathbf{A}\mathbf{x}'.$$

Thus Equation (28) becomes

$$\frac{\partial}{\partial \mathbf{x}} R = 2(s_h + \lambda_1 \rho_x) (\mathbf{x} - \mathbf{x}') + 2(\lambda_1 \mathbf{A} + \mathbf{H}^T \mathbf{H}) \mathbf{x}' - 2\mathbf{H}^T \mathbf{y}. \quad (29)$$

Setting Equation (29) to zero and solving for  $\mathbf{x}$  gives us our update term.

$$\mathbf{x} = \mathbf{x}' - \frac{1}{s_h + \lambda_1 \rho_x} (\lambda_1 \mathbf{A} + \mathbf{H}^T \mathbf{H}) \mathbf{x}' + \frac{1}{s_h + \lambda_1 \rho_x} \mathbf{H}^T \mathbf{y} \quad (30)$$

$$= \underbrace{\mathbf{x}' + \frac{1}{s_h + \lambda_1 \rho_x} \mathbf{H}^T (\mathbf{y} - \mathbf{H}\mathbf{x}')}_{\text{“Landweber term”}} - \underbrace{\frac{\lambda_1}{s_h + \lambda_1 \rho_x} \mathbf{A}\mathbf{x}'}_{\text{“TV term”}}. \quad (31)$$

Because this is an alternating minimization algorithm, we would repeat the above analysis in the same way for  $\mathbf{h}$ , arriving at the update for  $\mathbf{h}$  as

$$\mathbf{h} = \mathbf{h}' + \frac{1}{s_x + \lambda_1 \rho_h} \mathbf{X}^T (\mathbf{y} - \mathbf{X}\mathbf{h}') - \frac{\lambda_1}{s_x + \lambda_1 \rho_h} \mathbf{A}\mathbf{h}',$$

where  $s_x > \lambda_{\max}(\mathbf{X})$  and  $\rho_h > \lambda_{\max}(\mathbf{A}(\mathbf{h}))$ .

## 4. SIMULATIONS

In this section, we make performance comparisons between the AM algorithm, the TV algorithm derived in Section 3, and the TV *majorization-minimization* (MM) approach by Figuerido *et al.*<sup>12</sup> The images we used for comparison include a real-world image, which we took to be the classical cameraman image, a sparse image in the shape of a benzylbenzene molecule, and the Shepp-Logan phantom, which has smooth piecewise constant regions. In our simulations, we ran the AM and TV algorithms on each of the three noisy and blurred images, with  $\sigma = 0.2$ . In the blind TV algorithm, we initialized the estimate of the image using a Wiener filter as in the TV-MM algorithm.

Because we have motivated this paper based on MRFM, when we run the algorithms on the benzylbenzene image, we assumed the PSF, which we denote by  $\mathbf{H}^{\text{MRFM}}$ , to be an idealized two-dimensional realization of an MRFM PSF.  $\mathbf{H}^{\text{MRFM}}$  and  $\mathbf{H}_0^{\text{MRFM}}$  are depicted in Figure 3. We also considered the cylindrical out-of-focus blur shown in Figure 3(c), along with a Gaussian approximation of it in Figure 3(d), which we denote as  $\mathbf{H}^{\text{TV}}$  and  $\mathbf{H}_0^{\text{TV}}$ , respectively. Because the out-of-focus blur function is piecewise constant with discontinuities, it is well suited for the TV based algorithms.

In a simulation where we reconstructed the benzylbenzene molecule, we initialized each algorithm with the partially known PSF,  $\mathbf{H}_0^{\text{MRFM}}$ . We chose  $\lambda_1 = 0.01$  using the same method as the TV-MM algorithm implementation. For now, we empirically set  $\lambda_2 = 0.1$ . The parameters we used in the AM algorithm were also empirically chosen, with  $\gamma = 1000$ , and  $\lambda = 0.02$ . We ran the TV-MM algorithm for 50 iterations, the blind TV

algorithm for 5000 iterations, and the AM algorithm for 1000 iterations. The reconstruction results are shown in Figure 4. It is clear from these figures that AM performs a much better job. This is not surprising because the AM algorithm is specifically designed for this scenario by modeling sparsity in the image domain. We also depict each algorithm’s estimate of the true PSF. In the generation of Figure 4(e), we imposed a smoothing penalty of  $\tilde{\gamma} = 0.5$  after the completion of AM algorithm, using the ideas in Section 2.3. The AM algorithm is able to reconstruct a more accurate PSF than the blind TV algorithm. We stress that TV-MM is not a blind algorithm, and thus it does not recover a PSF.

For the reconstruction of the cameraman image, we downsampled the original image by a factor of four to a size of  $64 \times 64$  pixels in order to speed up computations. We also used total knowledge of the PSF,  $\mathbf{H}^{\text{TV}}$ , for this experiment. For the blind TV algorithm, we again set  $\lambda_1 = 0.27$  based on the final value of  $\lambda$  in the TV-MM algorithm. We also fixed the PSF to be the true PSF in the blind TV algorithm to try to match the performance of TV-MM. We allowed the TV algorithm to run for 10,000 iterations, while TV-MM ran for 50 iterations. It should be noted, however, that each iteration of the TV-MM algorithm may contain up to 200 conjugate gradient sub-iterations. We see from Figure 5, that both TV based algorithms perform similarly. TV-MM appears to have smoother regions than our TV algorithm, but some of the details in the background look sharper in Figure 5(b). The results shown for the AM algorithm are for 500 iterations. As expected, it performs poorly for this image.

Similarly, in reconstructing the Shepp-Logan phantom image with total knowledge of the PSF,  $\mathbf{H}^{\text{TV}}$ , both TV algorithms performed almost identically, with the blind TV algorithm running for 10,000 iterations, and TV-MM running for 50 iterations. We chose  $\lambda_1 = 0.22$  based on the final value of  $\lambda$  in the TV-MM algorithm. Reconstruction results are shown in Figure 6. The results for the TV algorithms are impressive, which makes sense since they are designed to deal with piecewise constant functions with discontinuities. Again, the AM algorithm ran for 500 iterations, and did not do well in recovering the image.

In another experiment, we tested our hypothesis that the blind TV algorithm should perform better for blind deconvolution problem versus the TV-MM algorithm. We used the Shepp-Logan phantom image, with  $\mathbf{H}_0^{\text{TV}}$  in Figure 3(d), running the TV-MM algorithm for 50 iterations, and running the blind TV algorithm for 100,000 iterations. We chose  $\lambda_1 = 0.22$ , as before, and empirically set  $\lambda_2 = 0.4$ . We tested on a  $64 \times 64$  image to speed up computations. Reconstruction results are shown in Figure 7. Visually, the results appear to be quite similar. On closer inspection, however, it appears the blind TV algorithm is able to clean up some ringing effects that appear around the reconstruction in 7(a), as well as creating smoother regions. The reconstruction results for the blind deconvolution are still rather dissatisfying, but we expect that further improvements can be made after exploring certain computational issues in the implementation of the algorithm. One explanation for the suboptimal reconstruction in Figure 7(c) is due to the fact that the piecewise constant image makes it difficult to estimate the PSF.

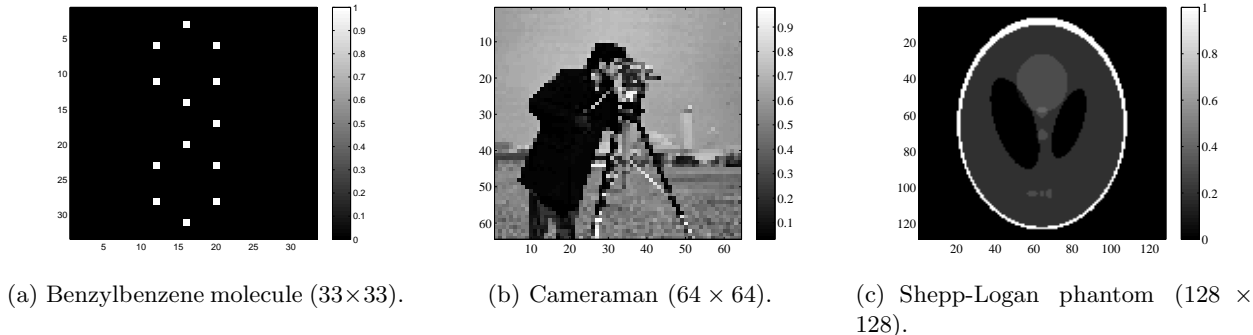
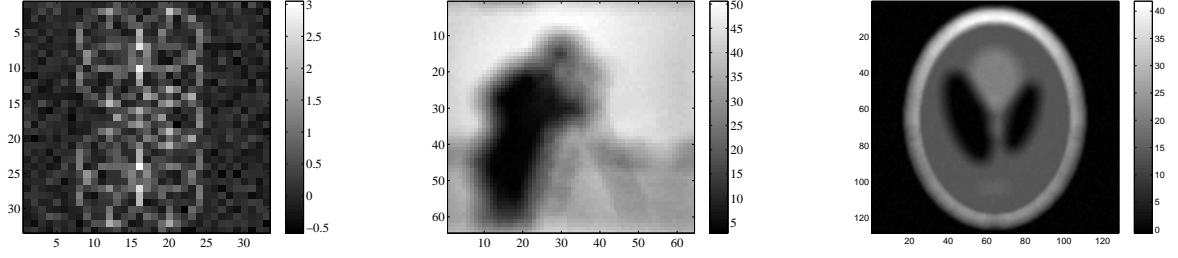


Figure 1. The three original images used.

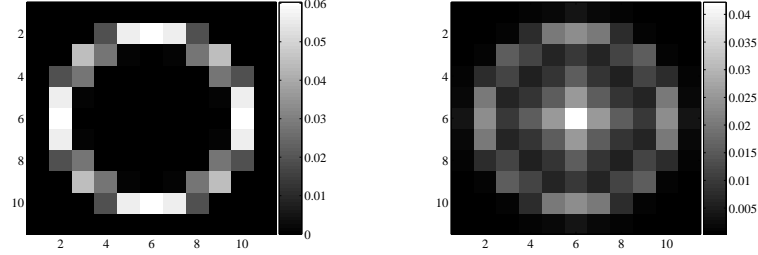
## 5. CONCLUSIONS AND FUTURE DIRECTIONS

This paper compares the performance of the AM algorithm, which models sparsity, versus a total variation alternating minimization algorithm. We demonstrated that better reconstruction results may be obtained with



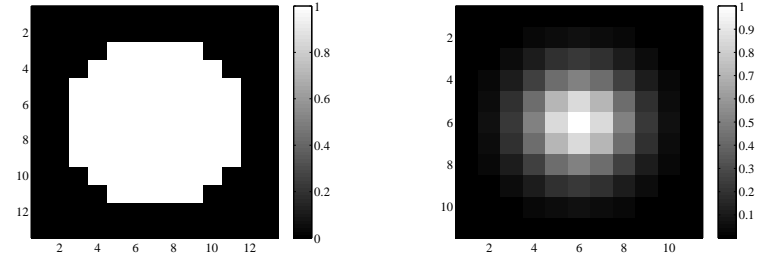
(a) Noisy and blurred benzylbenzene. (b) Noisy and blurred cameraman. (c) Noisy and blurred phantom.

Figure 2. The noisy and blurred images.



(a) Idealized MRFM PSF  $\mathbf{H}^{\text{MRFM}}$ .

(b) Approximate PSF  $\mathbf{H}_0^{\text{MRFM}}$ .



(c) True PSF  $\mathbf{H}^{\text{TV}}$ .

(d) Approximate PSF  $\mathbf{H}_0^{\text{TV}}$ .

Figure 3. The true PSFs used and their approximations.

the AM algorithm when the image is sparse, and when we use an appropriate partially known point spread function. For real world images, and in particular, for piecewise constant images, the TV based algorithms perform better than AM, as expected.

We observed that the blind TV deconvolution algorithm requires a large number of iterations in order to enjoy convergence, and when running on larger sized images, convergence rates become overwhelmingly slow. For example, for a  $128 \times 128$  image, the current implementation's utility becomes impractical. Further investigation into ways of speeding up the algorithm need to be explored. Also, we need to study efficient ways to select the regularization parameter values for  $\lambda_1$  and  $\lambda_2$  for a given image and initial PSF. Once these issues are resolved, it would be nice to extend these algorithms to handle three-dimensional images.

One possibility to explore would be to combine these optimization-transfer-based algorithms into a third algorithm by coupling the surrogate functions together. The disadvantage of such an approach, however, would be the added difficulty of a more complex parametrization for the regularization terms. Some other issues that still need to be explored include a more detailed analysis of each algorithm's convergence properties, as well as how to select the parameters in the AM algorithm to obtain the most satisfactory results.

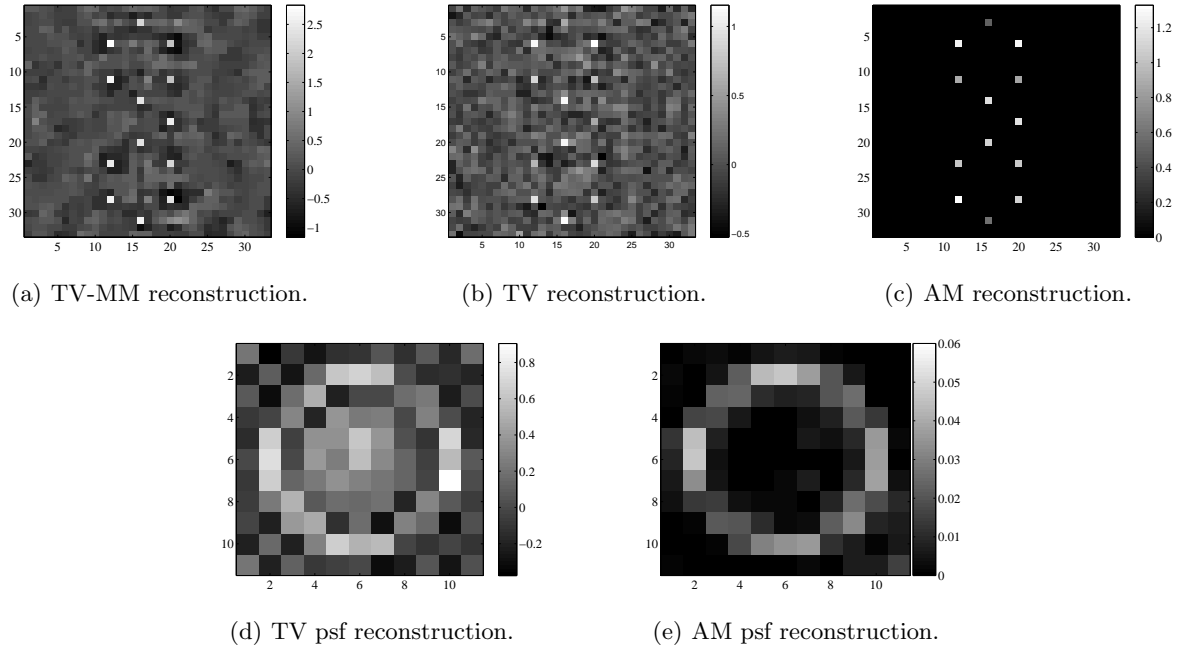


Figure 4. TV and AM reconstructions.

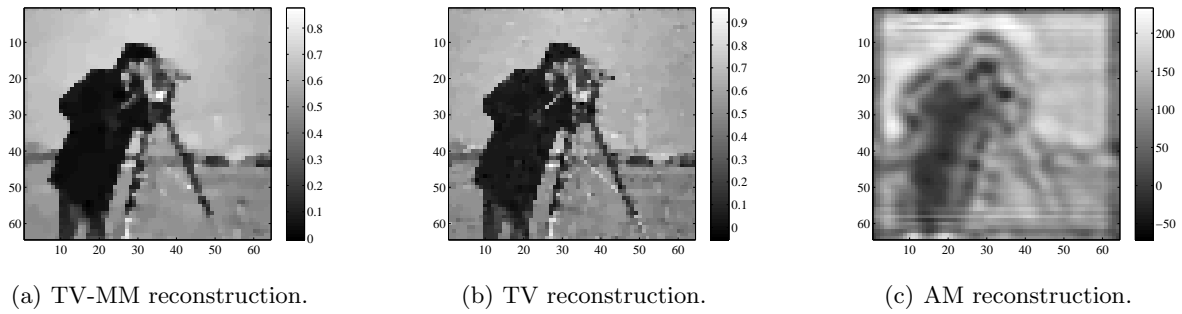


Figure 5. TV and AM reconstructions (with  $\mathbf{H}^{\text{TV}}$ ).

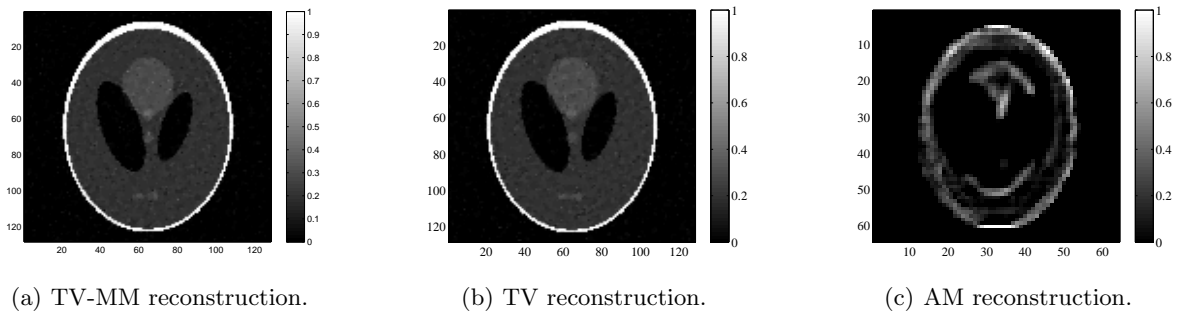


Figure 6. TV, TV-MM, and AM reconstructions (with  $\mathbf{H}^{\text{TV}}$ ).

## ACKNOWLEDGMENTS

This work is partially supported by the ARO MURI grant W911NF-05-1-0403.

## REFERENCES

1. H. Andrews and B. Hunt, *Digital Image Restoration*, Prentice-Hall, Englewood Cliffs, NJ, 1977.

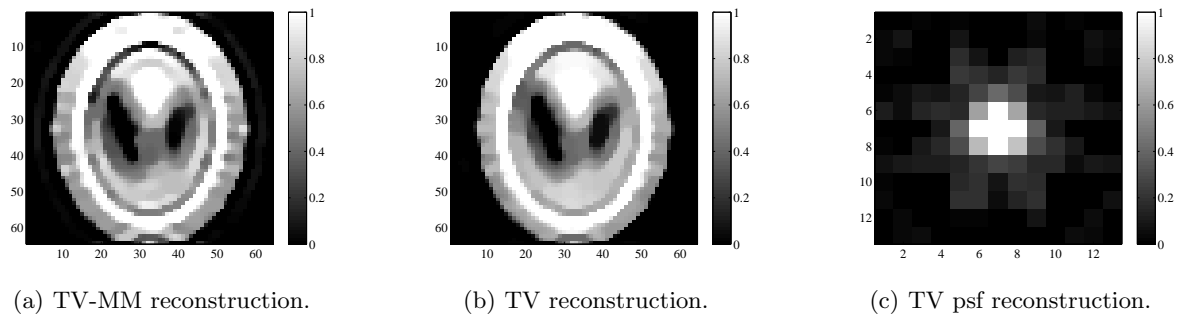


Figure 7. TV, TV-MM, and AM reconstructions (with  $\mathbf{H}_0^{\text{TV}}$ ).

2. J. Mamin, R. Budakian, and D. Rugar, “Point response function of an MRFM tip,” tech. rep., IBM Research Division, 2003.
3. M. Ting, *Signal Processing for Magnetic Resonance Force Microscopy*. PhD thesis, University of Michigan, May 2006.
4. K. Herrity, R. Raich, and A. O. Hero III, “Blind deconvolution for sparse molecular imaging.” Submitted to IEEE Intl Conf. on Acoustics, Speech and Signal Processing, April 2008.
5. T. Chan and C. Wong, “Total variation blind deconvolution,” *IEEE Transactions on Image Processing* **7**, pp. 370–375, March 1998.
6. J. Sidles and J. Garbini, “Program for achieving single nuclear spin detection,” tech. rep., University of Washington, 2006.
7. D. Rugar, R. Budakian, H. Mamin, and B. Chui, “Single spin detection by magnetic resonance force microscopy,” *Nature* **430**, pp. 329–332, July 2004.
8. G. Davis, S. Mallat, and M. Avellaneda, “Greedy adaptive approximation,” *J. Constr. Approx.* **13**, pp. 57–98, 1997.
9. B. Natarajan, “Sparse approximate solutions to linear systems,” *SIAM J. Comput.* **24**, pp. 227–234, 1995.
10. R. Raich and A. O. Hero III, “Sparse image reconstruction for partially unknown blur functions,” in *Proc. IEEE Int. Conf. Image Processing*, pp. 637–640, (Atlanta, GA), Oct. 2006.
11. M. A. T. Figueiredo and R. D. Nowak, “A bound optimization approach to wavelet-based image deconvolution,” in *Proc. IEEE Int. Conf. Image Processing*, **2**, pp. 782–785, Sept. 2005.
12. J. Bioucas-Dias, M. Figueiredo, and J. Oliveira, “Total variation image deconvolution: A majorization-minimization approach,” in *Proc. IEEE Intl. Conf. Acoust., Speech, Signal Processing*, **2**, pp. 861–864, (Toulouse, France), May 2006.